

Main Cause of the Poloidal Plasma Motion Inside a Magnetic Cloud Inferred from Multiple-Spacecraft Observations

Ake Zhao^{1,2,3}  · Yuming Wang^{1,4} · Yutian Chi^{1,3} ·
Jiajia Liu^{1,3} · Chenglong Shen^{1,4} · Rui Liu^{1,3}

Received: 25 February 2016 / Accepted: 3 March 2017 / Published online: 30 March 2017
© The Author(s) 2017. This article is published with open access at Springerlink.com

Abstract Although the dynamical evolution of magnetic clouds (MCs) has been one of the foci of interplanetary physics for decades, only few studies focus on the internal properties of large-scale MCs. Recent work by Wang *et al.* (*J. Geophys. Res.* **120**, 1543, 2015) suggested the existence of the poloidal plasma motion in MCs. However, the main cause of this motion is not clear. In order to find it, we identify and reconstruct the MC observed by the *Solar Terrestrial Relations Observatory* (STEREO)-A, *Wind*, and STEREO-B spacecraft during 19–20 November 2007 with the aid of the velocity-modified cylindrical force-free flux-rope model. We analyze the plasma velocity in the plane perpendicular to the MC axis. It is found that there was evident poloidal motion at *Wind* and STEREO-B, but this was not clear at STEREO-A, which suggests a local cause rather than a global cause for the poloidal plasma motion inside the MC. The rotational directions of the solar wind and MC plasma at the two sides of the MC boundary are found to be consistent, and the values of the rotational speeds of the solar wind and MC plasma at the three spacecraft show a rough correlation. All of these results illustrate that the interaction with ambient solar wind through viscosity might be one of the local causes of the poloidal motion. Additionally, we propose another possible local cause: the existence of a pressure gradient in the MC. The significant difference in the total pressure at the three spacecraft suggests that this speculation is perhaps correct.

Keywords Magnetic cloud · Poloidal plasma motion · Multiple-spacecraft observations · Rotational direction · Solar wind

✉ A. Zhao
zukeer@mail.ustc.edu.cn

Y. Wang
ymwang@ustc.edu.cn

- ¹ CAS Key Laboratory of Geospace Environment, Department of Geophysics and Planetary Sciences, University of Science and Technology of China, Hefei, Anhui 230026, China
- ² College of Physics and Electric Information, Luoyang Normal College, Luoyang, Henan 471934, China
- ³ Collaborative Innovation Center of Astronautical Science and Technology, Hefei 230026, China
- ⁴ Synergetic Innovation Center of Quantum Information and Quantum Physics, University of Science and Technology of China, Hefei, Anhui 230026, China

1. Introduction

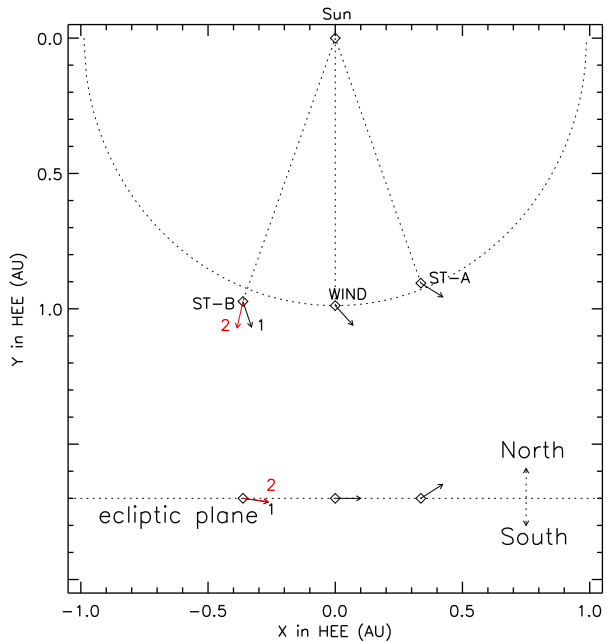
Magnetic clouds (MCs) as a considerable subset of interplanetary manifestations of coronal mass ejections (CMEs) have been studied for many years, since the first identification by Burlaga *et al.* (1981). The main reasons that we pay so much attention to MCs are that MCs have a relatively well-defined magnetic topology and are the main drivers for many space-weather events (*e.g.* Tsurutani *et al.*, 1988; Huttunen, Koskinen, and Schwenn, 2002; Wu and Lepping, 2002; Cane and Richardson, 2003; Zhang *et al.*, 2007). The dynamical evolution of MCs in interplanetary space is one of the important topics that need to be determined to improve the precision of space-weather forecasts.

Abundant observational evidence has shown that MCs may experience expansion (Burlaga and Behannon, 1982; Klein and Burlaga, 1982; Farrugia *et al.*, 1992, 1993; Lepping *et al.*, 2002; Wang, Du, and Richardson, 2005; Gulisano *et al.*, 2010), latitudinal and longitudinal deflection (Wang *et al.*, 2002, 2004, 2006a, 2014; Kilpua *et al.*, 2009; Rodriguez *et al.*, 2011; Isavnin, Vourlidas, and Kilpua, 2013), and/or rotation (Wang *et al.*, 2006b; Yurchyshyn, 2008; Yurchyshyn, Abramenko, and Tripathi, 2009; Vourlidas *et al.*, 2011; Nieves-Chinchilla *et al.*, 2012) when they propagate away from the Sun in the interplanetary medium. In addition to these motions, the “poloidal plasma motion” here refers to the motion of a velocity component along the poloidal direction, *i.e.*, around the MC axis, that has recently been found in the moving MC frame for many MCs by Wang *et al.* (2015). For this motion, the authors raised three possible explanations: i) it might be locally generated through the interaction with the solar wind; ii) it might be internally generated by the expansion of MCs, during which magnetic energy is converted into kinetic energy, including the rotational component; and iii) it might be initially generated at the eruption of the corresponding CME, and carried all the way to 1 AU.

In order to determine the main cause of the poloidal plasma motion in MCs, we employ multi-spacecraft observations to study the same MC. The *Solar Terrestrial Relations Observatory* (STEREO) has twin spacecraft, one (STEREO-A) leading and the other (STEREO-B) trailing the Earth, and the separation between them increases by about 45° per year (Kaiser *et al.*, 2008). The *in-situ* data from STEREO-A (ST-A), STEREO-B (ST-B), and the *Wind* spacecraft, which is at the Sun–Earth L_1 point, are often used to perform multi-spacecraft analyses. Nevertheless, the number of MCs that are suitable for a multi-spacecraft analysis is very limited, because when the distance between two spacecraft is too small (*e.g.* *Wind* and the *Advanced Composition Explorer* (ACE)), the two spacecraft observe almost identical structures; and when the distance between two spacecraft is too great, in addition to the finite longitudinal extent of the MC, which is about 60° (Wang *et al.*, 2011), the solar wind may also be strongly distorted, which means that it is difficult to recognize whether the structures belong to the same event. The separation angle between two STEREO spacecraft for a multipoint study is suggested to be no larger than $50\text{--}60^\circ$. We examined the MCs that occurred during February 2007 to June 2008, when the STEREO spacecraft were separated by about 1° to 58° , and we found that the best case for our study is the MC on 19 November 2007, when the spacecraft were separated by 41° .

In the next section, we identify and reconstruct the MC at the three spacecraft ST-A, *Wind*, and ST-B. In Section 3, we show evidence of the plasma poloidal motion in this MC and discuss the possible main cause of this motion. A conclusion is reached in Section 4.

Figure 1 The locations of the *Wind*, ST-A, and ST-B at 00:34 UT on 20 November 2007. The projected arrows on the ecliptic plane (top) and meridian plane (below) are the flux-rope axis derived from the velocity-modified force-free flux-rope model. Black: inferred from our identified MC at ST-B; red: the identified MC from Farrugia *et al.* (2011) at ST-B.



2. Data and Method

2.1. Data Source

The positions of the spacecraft at the occurrence of this event are shown in Figure 1. For ST-A and ST-B, the *in-situ* magnetic-field and solar-wind plasma data are obtained from the *In situ Measurements of Particles And CME Transients* (IMPACT: Luhmann *et al.*, 2008) and *Plasma and Suprathermal Ion Composition* (PLASTIC: Galvin *et al.*, 2008) instruments, and these are shown in Figures 2 and 4, respectively. Meanwhile, for *Wind*, the *in-situ* magnetic field and solar-wind plasma data from the *Magnetic Field Investigation* (MFI: Lepping *et al.*, 1995) and *Solar Wind Experiment* (SWE: Ogilvie *et al.*, 1995) instruments are shown in Figure 3. All magnetic-field strengths and plasma properties are plotted in one-minute temporal cadences, and the charge states of iron ions are averaged for two hours. The data of the average iron-ion charge state from the *Solar Wind Ion Composition Spectrometer* (SWICS: Gloeckler *et al.*, 1998) onboard ACE are used as a complement to the *Wind* data, because there is no instrument to measure the charge state of iron ions onboard *Wind*.

2.2. Identification of the MC at Three Spacecraft

This event was studied by Farrugia *et al.* (2011), Kilpua *et al.* (2011), and Ruffenach *et al.* (2012). The MC has different features than the ambient solar-wind properties when a spacecraft passes through the MC, including i) an enhanced magnetic field, ii) a smooth rotation over a large angle in the direction of the magnetic field, and iii) low proton β and temperature (Burlaga *et al.*, 1981; Klein and Burlaga, 1982). According to these three criteria, the MC was identified to last from 19 November, 22:30 UT to 20 November, 20:00 UT at ST-A, 20 November, 00:20–09:00 UT at *Wind*, and 19 November, 23:00 UT to 20 November, 07:00

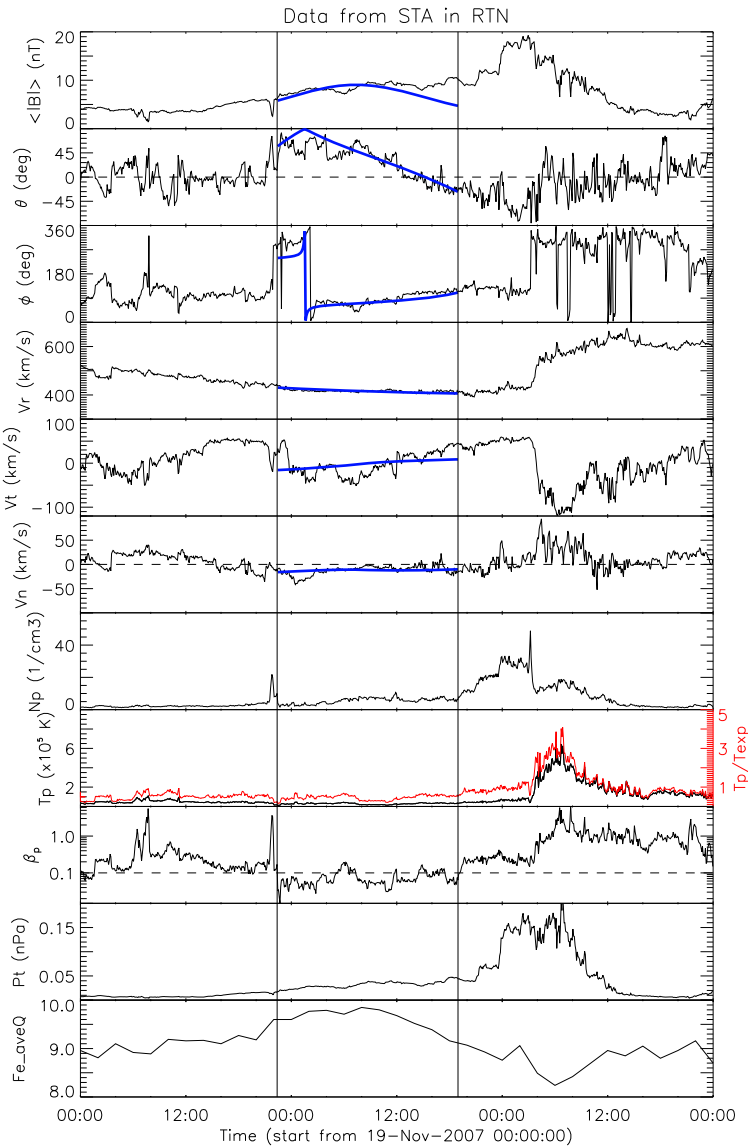


Figure 2 Interplanetary magnetic field and plasma data from ST-A. The two solid vertical lines indicate the boundary of the MC, and the blue curves (first to sixth panels) indicate the fitting results of our model. From top to bottom the panels are total magnetic-field strength [$\langle |B| \rangle$], elevation angle [θ], and azimuthal angle [ϕ] of the magnetic-field orientation, three components of the bulk velocity in RTN coordinate system, proton density [N_p], proton temperature [T_p], proton β_p , total pressure [P_t], and the average charge state of iron ions [F_e]. The ratio of the proton temperature to the expected proton temperature [T_p/T_{exp}] that is calculated based on the empirical formula from Lopez and Freeman (1986) is shown in the eighth panel by the red curve.

UT at ST-B in Farrugia *et al.* (2011). By comparing with the data at the three spacecraft, the authors found that the data at ST-B and *Wind* show a gradual transition from the slow to the fast solar wind, and ST-A may be located at the trailing edge of the previous high-speed

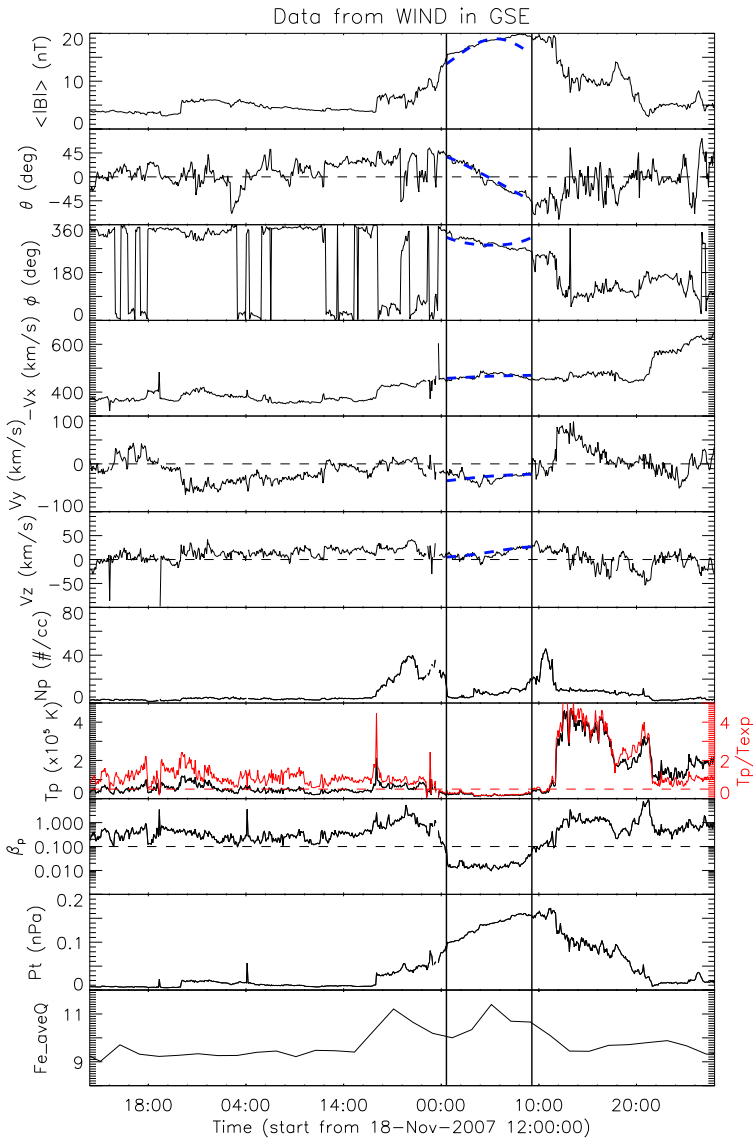


Figure 3 *In-situ* measurements (first to tenth panels) from *Wind* spacecraft and the charge state of iron ions (the eleventh panel) from the ACE spacecraft. The two solid lines indicate the boundary of the MC, and the blue dashed curves (first to sixth panels) indicate the fitting results of our model. From top to bottom the panels are the total magnetic-field strength [$|B|$], elevation angle [θ], and azimuthal angle [ϕ] of the magnetic-field orientation, three components of the bulk velocity in GSE coordinate system, proton density [N_p], proton temperature [T_p], proton β_p , total pressure [P_t], and the average charge state of iron ions [F_e]. The red curve in the eighth panel indicates the ratio of the proton temperature to the expected proton temperature [T_p/T_{exp}].

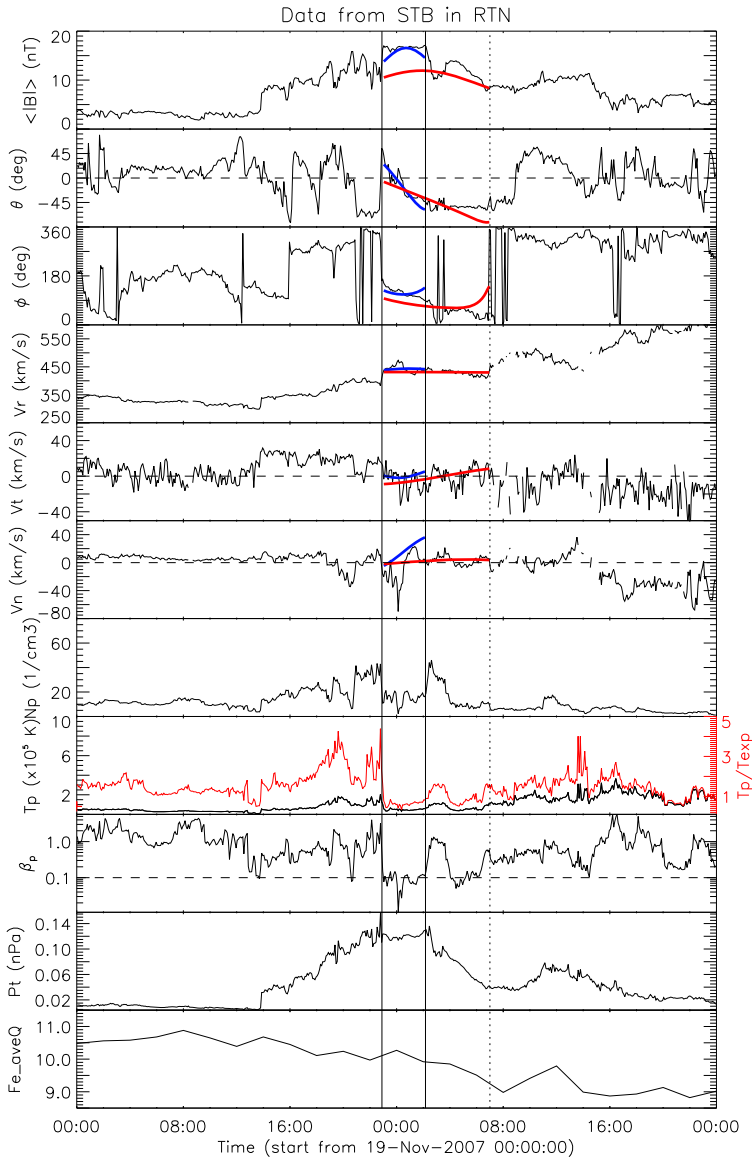


Figure 4 Interplanetary magnetic field and plasma data from ST-B. The MC region according to our identification result is marked by the two solid lines, and the region between the first solid line and the dotted line is derived from Farrugia *et al.* (2011). The blue and red curves (first to sixth panels) represent the fitting results of our model from our identification and that of Farrugia *et al.* (2011) separately. From top to bottom the panels are total magnetic-field strength [$\langle |B| \rangle$], elevation angle [θ], and azimuthal angle [ϕ] of the magnetic field orientation, three components of the bulk velocity in RTN coordinate system, proton density [N_p], proton temperature [T_p], proton β_p , total pressure [P_t], and the average charge state of iron ions [F_c]. The red curve in the eighth panel indicates the ratio of the proton temperature to the expected proton temperature [T_p/T_{exp}].

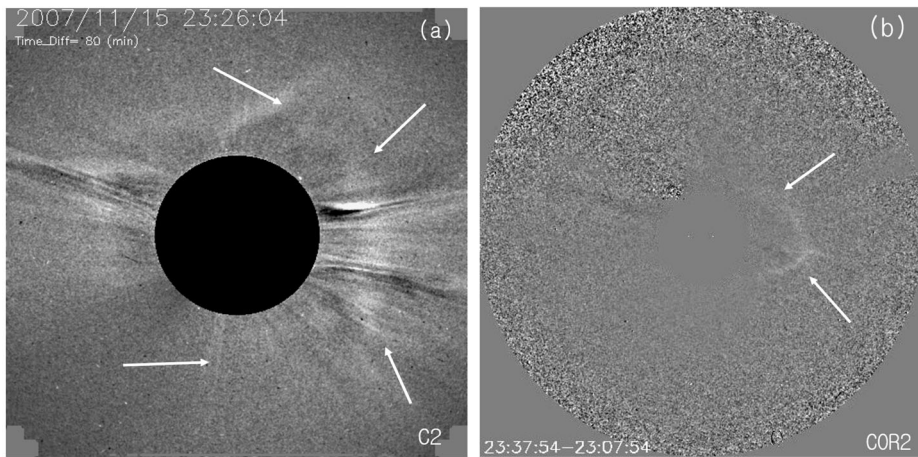


Figure 5 Observations of the CME on 15 November 2007 from the coronagraphs. (a) The running-difference SOHO/LASCO-C2 image, and (b) the running-difference ST-B/COR2 image.

solar wind. The identified boundaries of the MC are almost the same in the other two articles (Kilpua *et al.*, 2011; Ruffenach *et al.*, 2012).

By combining the above three classic signatures of an MC and the features in the density and iron charge state, we make our own identification of the boundaries of the MC at the three spacecraft. Our identified boundaries of the MC at ST-A and *Wind* are quite similar to those by Farrugia *et al.* (2011). At ST-A, the MC in our view started at 19 November, 22:25 UT and ended at 19:00 UT on the next day (see Figure 2), which is five minutes and one hour earlier than the leading and trailing edge identified by Farrugia *et al.* (2011). At *Wind*, the MC we identified started on 20 November, 00:30 UT and ended at 09:20 UT (see Figure 3), which is 10 minutes and 20 minutes later than the leading and trailing edge identified by Farrugia *et al.* (2011). At ST-B, the MC boundaries suggested by Farrugia *et al.* (2011) are marked by the first solid line and the dotted line (see Figure 4). There is a high-density region in the middle of the MC, which was regarded as filament material contained within the MC (Farrugia *et al.*, 2011). However, we note that a similar high-density region appeared after the trailing edge of the MC in both ST-A and *Wind* observations. We therefore propose here a different scenario: the MC at ST-B was located between the two solid lines, as shown in Figure 4, in which the high-density region followed the MC, just like those observed at ST-A and *Wind*. Moreover, the profile of the average charge state of iron ions at ST-B shows that the charge state first reached a peak inside the MC and then decreased to a low outside the MC in our identification. This is consistent with the measurements at both ST-A and *Wind*. Although we proposed a rear boundary different from that by Farrugia *et al.* (2011) for the MC at ST-B, it is difficult to judge which identification is more correct. We therefore consider both possibilities in the following analysis. Hereafter, we use ST-B for our identification and ST-B' for the identification of Farrugia *et al.* (2011).

According to the velocity (about 450 km s^{-1}) of the *in-situ* MC at *Wind*, the source CME can be roughly estimated to have launched on 15 November 2007. After searching in the online LASCO CME catalog (Yashiro *et al.*, 2004), we found that there is no suitable CME from 14 to 16 November except for the faint partial halo CME that erupted around 18:50 UT on 15 November, as shown in Figure 5a. This CME can also be seen from ST-B, as shown in Figure 5b. We conclude that it is the source of the MC. However, the exact source region cannot be identified confidently because of the weak activity on the solar surface.

2.3. Reconstruction of the MCs

We used the velocity-modified cylindrical force-free flux-rope model that was developed by Wang *et al.* (2015) to fit the MC. For ST-A and ST-B, we show the measurements in the RTN coordinate system, in which R points from the Sun to the spacecraft, T is perpendicular to R and points in the direction of planetary motion, and N completes the right-hand coordinate system. For *Wind*, the GSE coordinate system was used. Meanwhile, a cylindrical coordinate system (r, φ, z) and a Cartesian coordinate system (x', y', z') were used to present the data in the MC frame, which were illustrated in detail in Wang *et al.* (2015). The axis orientation of the flux-rope is indicated by the elevation and azimuthal angles θ and ϕ . When $\theta = 0$, the axis is in the ecliptic plane, and $\theta = 0$ and $\phi = 0$ means that the axis points to the Sun in GSE coordinates or to the spacecraft in RTN coordinates. By considering the linear propagating motion [v_c], the expanding motion [v_e], and the poloidal motion [v_p], the model not only uses three components of the measured magnetic field, but also three components of the measured velocity to constrain the fitting parameters.

In the light of the boundary of the MC at three spacecraft that we identified, we use our model to fit the five-minute-averaged data of the MC. All of the fitting parameters obtained by the model are shown in Table 1, and the fitting results are indicated by the blue lines in Figures 2–4. We also fit to the MC at ST-B according to the boundary of Farrugia *et al.* (2011) and show this as the red line in Figure 4.

Our fitting results of the MC at the three spacecraft are roughly consistent with those given by Farrugia *et al.* (2011). The largest difference occurs in the orientation of the MC axis. At *Wind*, the orientation difference is about 40–50°, while at ST-A and ST-B the difference is smaller than 20°. The orientation of the MC at the three spacecraft is plotted in Figure 1. From this figure, it is clear that the axes of the MC at the three spacecraft roughly align along a loop, in agreement with the common picture of an MC that is a globally loop-like structure with two ends rooted on the Sun.

From Table 1, the parameter d , *i.e.* the closest approach, at ST-B and *Wind* is about 0.75–0.85, which means that the spacecraft crossed the edge of the MC, which perhaps affects the reliability of our model results. Riley *et al.* (2004) performed “blind tests” for a magnetohydrodynamically (MHD) simulated MC using five different fitting techniques, and they found that a large deviation for the orientation of the MC axis existed, especially when the closest approach of the spacecraft to the MC axis is large. However, in the three types of linear force-free models, the orientation of the MC axis from Lepping’s model (Lepping, Burlaga, and Jones, 1990) is closest to the value that the MHD model gave, in which the difference is less than 60°. Our model has been demonstrated statistically to yield similar fitting results as Lepping’s linear force-free flux-rope model (Wang *et al.*, 2015). In this study, we assume that the modeled orientations are close to the real orientations, and we investigate the poloidal motion of the MC plasma in the following sections.

3. Poloidal Motion Inside the MC at Different Spacecraft

After we obtained the orientation of the MC axis, we converted the magnetic field and velocity into the MC frame, (x', y', z') , in which z' is along the axis of the MC that is perpendicular to the $x'-y'$ plane. The thick black arrows in Figures 6d–8d show the paths along which the spacecraft pass through the MC projected on the $x'-y'$ plane. Along the path from the beginning to the end of the MC, the observed x' - and y' -components of the magnetic field and plasma velocity are shown by color-coded dots in Figures 6a, b–8a, b. A clear and regular

Table 1 The fitting parameters of the MC obtained by the velocity-modified cylindrical force-free flux-rope model.

Spacecraft	MC interval	Modeled parameters ^a												
		B_0	R	H	θ	ϕ	d	v_X	v_Y	v_Z	v_e	v_p	Δt_c	X_n
ST-A (RTN)	19 Nov 2007 22:25 – 20 Nov 2007 19:00	10	0.09	-1	31	39	-0.40	420	0	-20	18	-7	9.8	0.42
Wind (GSE)	20 Nov 2007 00:30 – 20 Nov 2007 09:20	28	0.05	-1	0	222	-0.75	-455	-38	26	-15	16	4.5	0.23
Wind (RTN)					0	42		455	38	26				
ST-B (RTN)	19 Nov 2007 23:00 – 20 Nov 2007 02:10	27	0.02	-1	-8	40	-0.84	418	28	14	-7	38	1.6	0.23
ST-B' (RTN)	19 Nov 2007 23:00 – 20 Nov 2007 07:00 ^b	18	0.01	-1	-7	7	-0.78	429	4	-9	6	13	3.8	0.42

^aAll of the parameter symbols and units are the same as those in Wang *et al.* (2015).

^bInterval from Farrugia *et al.* (2011).

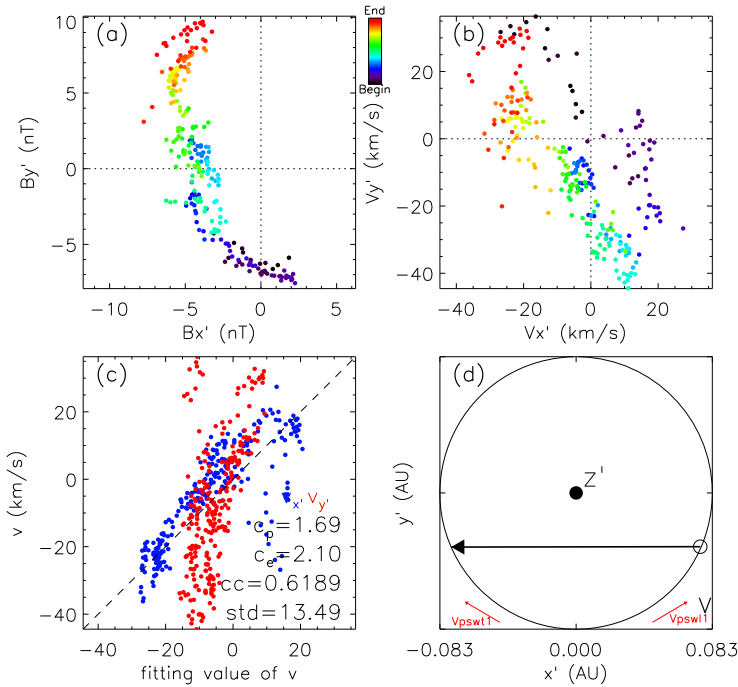


Figure 6 Measurements from ST-A in the $x'-y'$ plane of the MC frame. (a) Observed magnetic field and (b) observed plasma velocity inside the MC. Different color means different time from the front boundary to the rear boundary of the MC, as indicated by the color bar beside panel a. (c) Scatter plot of the measured velocity *versus* the fitted velocity inside the MC. (d) The cross-section of the MC. The black arrow denotes the observational path. The tangential component of the solar-wind velocity outside the MC is indicated by the red arrows.

arc-structure is found in the magnetic-field data (see Figure 6a–8a), confirming the helical magnetic structure in the MC. In Figures 7b–8b, we can also find an arc-like distribution of the velocity in the $x'-y'$ plane, which indicates the poloidal motion of the plasma flow inside the MC. For the MC observed by *Wind*, this motion rotates anticlockwise, with the velocity changing from $+v_{y'}$ to $+v_{x'}$. The signature of the poloidal motion for the MC observed by ST-B is not as clear as that observed by the *Wind* spacecraft, but it can still be recognized as an anticlockwise rotation in the $x'-y'$ plane. For the MC observed by ST-A, there is no clear plasma rotation. We also analyzed the poloidal motion inside the MC at ST-B with the boundary identified by Farrugia *et al.* (2011) (Figure 9), and the poloidal motion was also very weak. The modeled overall poloidal velocities are listed in Table 1.

To further check the reliability of our model results, we used the equation

$$v_t = c_p \mathbf{B}_t + c_e \mathbf{b}'_t,$$

$$\mathbf{b}'_t = \begin{pmatrix} 0 & -1 \\ 1 & 0 \end{pmatrix} \mathbf{B}_t / |\mathbf{B}_t|,$$

where c_p and c_e are two free parameters, \mathbf{B}_t is the measured magnetic field in the $x'-y'$ plane to fit the measured velocity $[v_t]$ in the $x'-y'$ plane. Here, we consider that the magnetic field is a well-organized helical structure and the plasma is frozen on the magnetic-field lines,

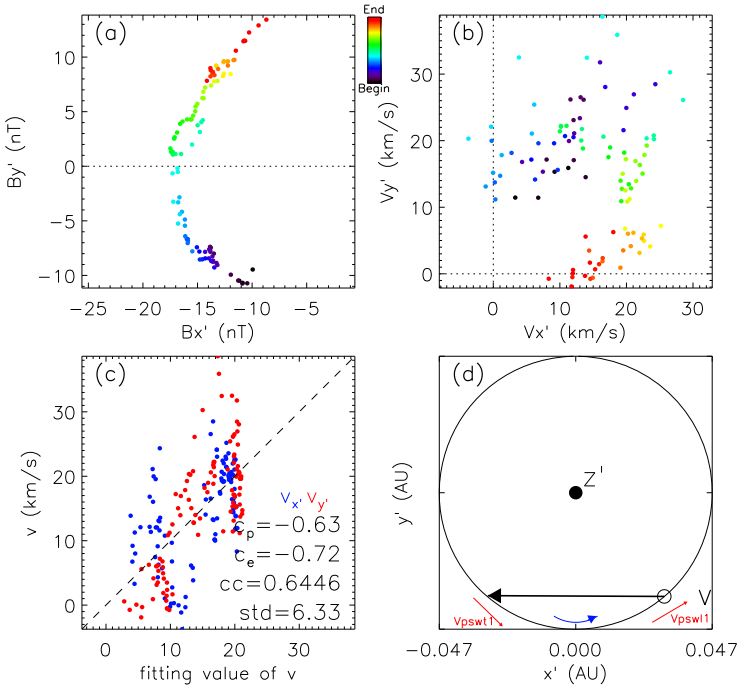


Figure 7 Measurements from *Wind* in the x' - y' plane of the MC frame. (a) Observed magnetic field and (b) observed plasma velocity inside the MC. Different color means different time from the front boundary to the rear boundary of the MC, as indicated by the color bar beside panel a. (c) Scatter plot of the measured velocity *versus* the fitted velocity inside the MC. (d) The cross-section of the MC. The black arrow denotes the observational path. The tangential component of the solar-wind velocity outside the MC is indicated by the red arrows. The poloidal component of the MC plasma velocity inside the MC is indicated by the blue arrow.

therefore v_i is decomposed into two components, *i.e.* poloidal motion and expansion, which are assumed to be parallel and perpendicular to the local magnetic-field line, respectively. Figures 6c–9c show the results. The horizontal axis indicates the fitted velocity, which is calculated from the above formula based on the measured \mathbf{B} after c_p and c_e are obtained from the fitting to all the data points, and the vertical axis represents the measured velocity. The blue dots represent the $v_{x'}$ -component of the velocity, and the red dots represent the $v_{y'}$ -component.

Significant correlations are found between the fitting and measured velocities at all the three spacecraft. The correlation coefficients are 0.6189, 0.6446, 0.6359, and 0.6959 at ST-A, *Wind*, ST-B, and ST-B', respectively. This suggests that the velocity model incorporated in our flux-rope forward-modeling is reasonable and acceptable, and the significant deviation might result from fluctuations in the measured magnetic field and velocity, and it reveals why this poloidal motion of the plasma inside MCs was not noted before.

We have given three hypotheses for the causes of the poloidal motion (Wang *et al.* 2015; see also the Introduction). Two of them are global reasons, which should cause a consistent poloidal motion at the three spacecraft. The above analysis has suggested anticlockwise rotation at *Wind* and ST-B, but no clear rotation at ST-A. This implies that the main cause of the poloidal motion cannot be global, but must be local. We note that even if we had

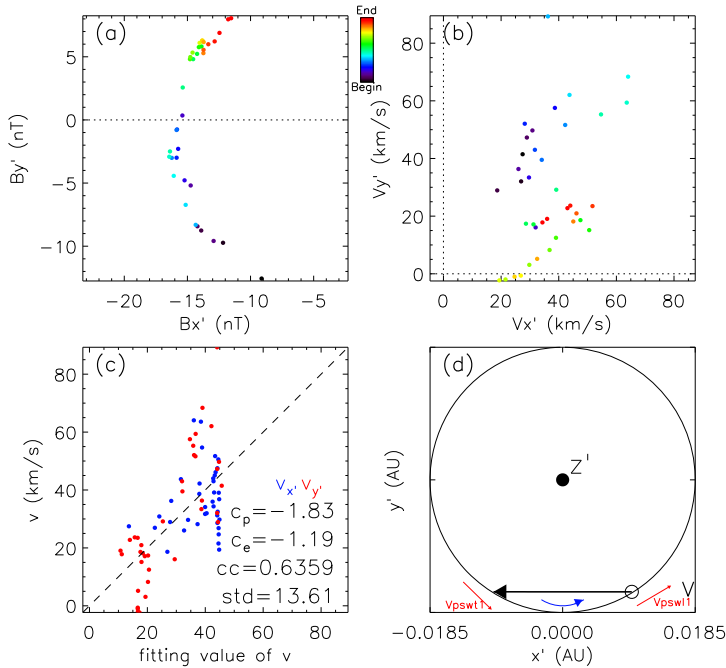


Figure 8 Measurements from ST-B identified by us in the x' - y' plane of the MC frame. (a) Observed magnetic field and (b) observed plasma velocity inside the MC. Different color means different time from the front boundary to the rear boundary of the MC, as indicated by the color bar beside panel a. (c) Scatter plot of the measured velocity *versus* the fitted velocity inside the MC. (d) The cross-section of the MC. The black arrow denotes the observational path. The tangential component of the solar-wind velocity outside the MC is indicated by the red arrows. The poloidal component of the MC plasma velocity inside the MC is indicated by the blue arrow.

replaced ST-B with ST-B', the conclusion would not be changed as the poloidal motion was quite different at the three spacecraft.

What type of local process may cause this poloidal motion inside the MC? One possible process is the interaction with the ambient solar wind. Viscosity is an intrinsic property of the solar wind (e.g. Whang, Liu, and Chang, 1966; Hundhausen, 1968; Hollweg, 1978; Bruno and Carbone, 2005). As long as there is a velocity difference between the MC plasma and the ambient solar wind at the boundary of the MC, the poloidal motion probably has a natural cause. To check this speculation, we first calculated the average solar-wind velocity every 15 minutes before the leading and after the trailing edge in the x' - y' plane. The values of the velocity component tangential to the modeled MC boundary (labeled v_{pswti} and v_{pswti} , $i = 1, 2$ and 3, with the smaller number indicating a place closer to the MC boundary) are listed in Table 2, in which the positive number means the anticlockwise rotation and the negative number the clockwise rotation. The uncertainty is the standard deviation of the speed in the 15-minute interval. Second, we calculated the average tangential plasma velocities within the MC every 15 minutes after the leading and before the trailing edge [v_{pt1} , v_{pt2} , v_{pt3} , v_{pt2} , and v_{pt1}] which are also listed in Table 2.

The tangential velocities of the solar wind closest to the MC boundary are marked by the red arrows in Figures 6d–9d. From Figures 7d and 8d, we find that the rotational directions of the tangential velocities [v_{pswt1} and v_{pswt1}] are consistent at *Wind* and ST-B, where the

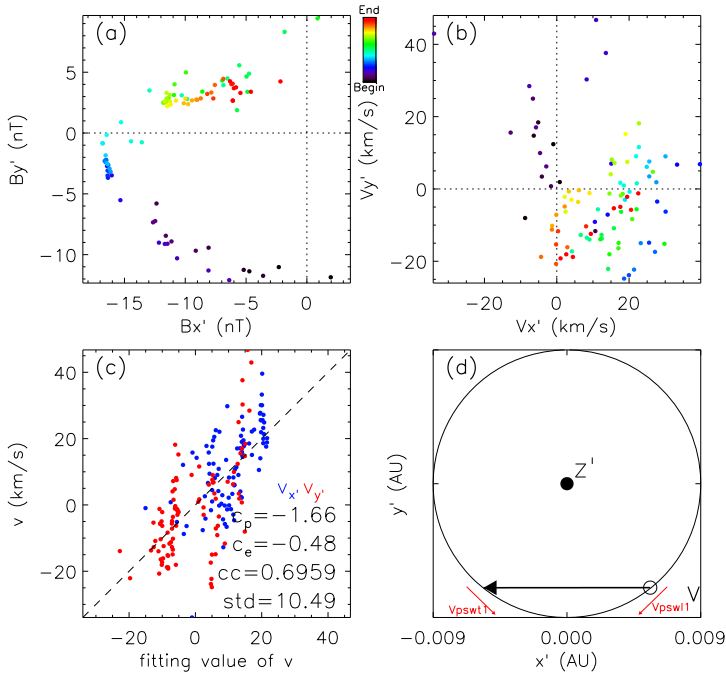


Figure 9 Measurements from ST-B identified from Farrugia *et al.* (2011) in the x' - y' plane of the MC frame. (a) Observed magnetic field and (b) observed plasma velocity inside the MC. Different color means different time from the front boundary to the rear boundary of the MC, as indicated by the color bar beside panel a. (c) Scatter plot of the measured velocity versus the fitted velocity inside the MC. (d) The cross-section of the MC. The black arrow denotes the observational path. The tangential component of the solar-wind velocity outside the MC is indicated by the red arrows.

plasma poloidal motions inside the MC are significant. However, at ST-A the rotations of the ambient solar wind near the front and rear boundaries were opposite, as illustrated in Figure 6d. The rotations of the MC plasmas near the front and rear boundaries were also opposite (see Table 2). This is probably the reason why the modeled overall poloidal speed is not evident. We note, however, that the rotational direction inside the MC is consistent with the rotational direction of the ambient solar wind at both the front and rear boundaries. The situation at ST-B' is similar. This apparent relationship between the rotational directions of the solar-wind plasma and the MC plasma qualitatively supports the idea that the interaction between the solar wind and the MC might be a cause of the poloidal plasma motion inside the MC.

To further quasi-quantitatively investigate the interaction between the solar wind and MC, we show the relation between the $(v_{pswi} + v_{pswi})/2$ and $(v_{pli} + v_{pti})/2$, where i is equal to 1, 2, and 3 in Figure 10. We use the sum of the tangential speeds at the front and rear boundaries to reduce possible local bias and uncertainties and show an overall relation of the plasma velocities at the two sides of the MC boundary. The error bars in Figure 10 are the mean value of the errors of the velocities at the front and rear boundaries. From the left panel to the right panel, the data points used in the plot move farther from the boundary of the MC. These panels show that the tangential velocities at the two sides of the MC boundary are roughly correlated. Considering the possible uncertainty in identifying the boundary of the MC, the correlations presented in the plots are expected to become more and more reliable

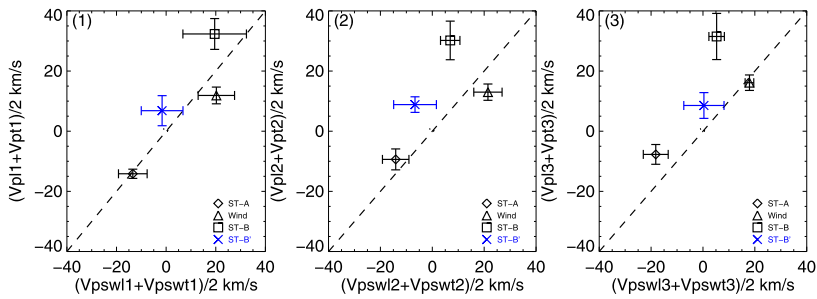


Figure 10 Relation between the $(v_{pswli} + v_{pswti})/2$ and $(v_{pli} + v_{pti})/2$ obtained from Table 2. From left to right, the three panels represent the data points ($i = 1, 2, 3$).

from the left panel to the right. The signs of $v_{pswli} + v_{pswti}$ and $v_{pli} + v_{pti}$ are consistent with each other at ST-A, *Wind*, and ST-B in all of the three panels, except for that at ST-B'.

In particular, the middle and right panels show that the rotational speeds of the ambient solar wind are higher overall than those of the MC plasma at ST-A and *Wind*, suggesting that the viscosity may affect the poloidal motion. However, the data point at ST-B does not follow this pattern. Furthermore, the tangential velocity does not show a clear pattern that the value decreases from the edge of the MC toward the axis of the MC. These inconsistencies imply that the interaction with the solar wind through viscosity might be only one of the local causes of the poloidal motion. Here we propose another possible cause: a pressure gradient in the MC. An MC is a large-scale structure in interplanetary space. Its interaction with ambient solar wind cannot be uniform everywhere. In other words, the different parts of the MC may be affected by the solar wind to different degrees, and therefore the local pressures inside the MC may be non-uniform, which might also lead to local poloidal motion following the helical magnetic-field lines. However, this scenario is difficult to examine. One preliminary preparation to aid this verification is to check the total pressure at the three spacecraft, which is plotted in the second panels from the bottom of Figures 2–4. They show that the total pressures in the MC at the three spacecraft are different, perhaps confirming this speculation.

4. Summary and Conclusion

In this article, multi-spacecraft observations were employed to study the possible main reason that causes the poloidal plasma motion inside the MC that was observed by ST-A, *Wind*, and ST-B during 19–20 November 2007, when the separation of ST-A and ST-B was about 41° . With the aid of the velocity-modified force-free flux-rope model, we reconstructed the MC and found a significant poloidal plasma motion inside the MC at *Wind* and ST-B in the plane perpendicular to the MC axis. At *Wind* and ST-B it is anticlockwise, but there is no clear poloidal motion at ST-A and ST-B'. The different poloidal motion at different spacecraft suggests that the main cause of the poloidal motion is not global, but local.

We then checked the possible local cause, which we hypothesize is the interaction between the solar-wind plasma. By calculating the measured tangential velocities of the ambient solar wind and the MC plasma at the two sides of the MC boundary in the MC frame, we find that the rotational direction of the solar wind is consistent with the modeled overall poloidal motion. Furthermore, we compared the values of the tangential velocities,

Table 2 The poloidal component of the averaged velocity in the $x'-y'$ plane of the MC frame.

Spacecraft	v_{psw13}	v_{psw12}	v_{psw11}	v_{p11}	v_{p12}	v_{p13}	v_{pt2}	v_{pt1}	v_{pswt1}	v_{pswt2}	v_{pswt3}
ST-A	-9.74 ± 5.39	6.16 ± 8.71	9.03 ± 10.04	9.09 ± 1.48	20.00 ± 3.81	21.70 ± 4.67	-37.12 ± 1.90	-38.73 ± 3.14	-35.89 ± 1.58	-34.38 ± 1.52	-26.66 ± 4.21
Wind	22.01 ± 0.50	24.31 ± 2.85	18.34 ± 6.90	14.66 ± 4.03	17.44 ± 3.54	23.82 ± 3.25	8.44 ± 1.89	8.53 ± 1.88	22.14 ± 1.53	18.59 ± 8.04	13.83 ± 2.83
ST-B	-1.30 ± 2.42	-8.42 ± 3.29	16.97 ± 22.69	40.67 ± 8.79	42.56 ± 10.41	43.99 ± 14.76	18.99 ± 0.57	17.80 ± 2.43	23.98 ± 1.47	22.24 ± 4.19	11.83 ± 3.54
ST-B'	-12.36 ± 11.69	-15.09 ± 13.61	-7.62 ± 9.98	0.10 ± 9.04	2.49 ± 4.62	1.76 ± 6.23	15.34 ± 2.34	15.20 ± 0.55	13.54 ± 0.96	4.38 ± 6.84	1.77 ± 2.86

Note: The averaged poloidal velocity of the solar-wind plasma before the leading and after the trailing edge of the MC [v_{pswt1} and v_{pswt2}], and the averaged poloidal tangential plasma velocities every 15 minutes inside the MC (near the leading edge: v_{p1} ; near the trailing edge: v_{p2}). Negative number means clockwise rotation and positive number means anticlockwise rotation. The data at ST-B' are obtained from the MC region in Farrugia *et al.* (2011).

$(v_{\text{pswli}} + v_{\text{pswti}})/2$ and $(v_{\text{pli}} + v_{\text{pti}})/2$ ($i = 1, 2$ and 3), at the three spacecraft and derived a rough correlation between them (see Figure 10). These results illustrate that the solar wind might be able to cause the poloidal motion in the MC through viscosity. The strength of the viscosity mainly depends on the gradient of the velocity and may be modified by the magnetic field in magnetized plasmas (*e.g.* Hollweg, 1985). The importance of viscosity in the solar wind has been demonstrated in the studies of CME's dynamical evolution, *e.g.* the aerodynamic drag force is a manifestation of the viscosity, which may dominant the dynamic evolution of ICMEs in interplanetary space (*e.g.* Subramanian, Lara, and Borgazzi, 2012; Vršnak *et al.*, 2013; Hess and Zhang, 2015). Here our study suggests, from another point of view, that the viscosity plays a significant role in some circumstances. The question now is how the viscosity takes effect in a collisionless plasma. More work is necessary to address this issue.

However, in the above picture, the tangential speed of the solar wind should be higher than that inside the MC, which is roughly true at ST-A and *Wind*, but not at ST-B. Moreover, the viscosity should cause the tangential velocity to be higher at the edge than in the inner part of the MC. However, no such pattern is evident in our study. These inconsistencies imply that there are probably other local reasons causing the poloidal motion. By briefly checking the total pressure inside the MC at the three spacecraft, we propose that the nonuniform pressure in the large-scale MC structure might be another local cause.

We note that the conclusions obtained in this article are based on only one case, which needs to be verified by more events in future work.

Acknowledgements We acknowledge use of data from STEREO, ACE, and *Wind*. This research is supported by NSFC (41131065, 41574165, 41421063, 41274173, 41222031), CAS (Key Research Program KZZD-EW-01 and 100-Talent Program), and the fundamental research funds for the central universities.

Disclosure of Potential Conflicts of Interest The authors declare that they have no conflicts of interest.

Open Access This article is distributed under the terms of the Creative Commons Attribution 4.0 International License (<http://creativecommons.org/licenses/by/4.0/>), which permits unrestricted use, distribution, and reproduction in any medium, provided you give appropriate credit to the original author(s) and the source, provide a link to the Creative Commons license, and indicate if changes were made.

References

- Bruno, R., Carbone, V.: 2005, The solar wind as a turbulence laboratory. *Living Rev. Solar Phys.* **2**(1), 1. [DOI](#)
- Burlaga, L.F., Behannon, K.W.: 1982, Magnetic clouds – Voyager observations between 2 and 4 AU. *Solar Phys.* **81**, 181. [DOI](#)
- Burlaga, L., Sittler, E., Mariani, F., Schwenn, R.: 1981, Magnetic loop behind an interplanetary shock – Voyager, Helios, and IMP 8 observations. *J. Geophys. Res.* **86**, 6673. [DOI](#)
- Cane, H.V., Richardson, I.G.: 2003, Interplanetary coronal mass ejections in the near-Earth solar wind during 1996–2002. *J. Geophys. Res.* **108**, 1156. [DOI](#)
- Farrugia, C., Burlaga, L., Osherovich, V., Lepping, R.: 1992, A comparative study of dynamically expanding force-free, constant-alpha magnetic configurations with applications to magnetic clouds. In: Marsch, E., Schwenn, R. (eds.) *Solar Wind Seven Coll.*, Pergamon, New York, 611.
- Farrugia, C., Burlaga, L., Osherovich, V., Richardson, I., Freeman, M., Lepping, R., Lazarus, A.: 1993, A study of an expanding interplanetary magnetic cloud and its interaction with the Earth's magnetosphere: The interplanetary aspect. *J. Geophys. Res.* **98**(A5), 7621. [DOI](#)
- Farrugia, C., Berdichevsky, D., Möstl, C., Galvin, A., Leitner, M., Popecki, M., Simunac, K., Opitz, A., Lavraud, B., Ogilvie, K., *et al.*: 2011, Multiple, distant (40) in situ observations of a magnetic cloud and a corotating interaction region complex. *J. Atmos. Solar-Terr. Phys.* **73**(10), 1254.
- Galvin, A., Kistler, L., Popecki, M., Farrugia, C., Simunac, K., Ellis, L., Möbius, E., Lee, M., Boehm, M., Carroll, J., *et al.*: 2008, The Plasma and Suprathermal Ion Composition (PLASTIC) investigation on the STEREO observatories. *Space Sci. Rev.* **136**(1–4), 437. [DOI](#)

- Gloeckler, G., Cain, J., Ipavich, F.M., Tums, E.O., Bedini, P., Fisk, L.A., Zurbuchen, T.H., Bochsler, P., Fischer, J., Wimmer-Schweingruber, R.F., Geiss, J., Kallenbach, R.: 1998, Investigation of the composition of solar and interstellar matter using solar wind and pickup ion measurements with SWICS and SWIMS on the ACE spacecraft. *Space Sci. Rev.* **86**, 497. DOI
- Gulisano, A., Démoulin, P., Dasso, S., Ruiz, M., Marsch, E.: 2010, Global and local expansion of magnetic clouds in the inner heliosphere. *Astron. Astrophys.* **509**, A39.
- Hess, P., Zhang, J.: 2015, Predicting CME ejecta and sheath front arrival at L1 with a data-constrained physical model. *Astrophys. J.* **812**(2), 144. DOI
- Hollweg, J.V.: 1978, Some physical processes in the solar wind. *Rev. Geophys.* **16**(4), 689. DOI
- Hollweg, J.V.: 1985, Viscosity in a magnetized plasma: Physical interpretation. *J. Geophys. Res.* **90**(A8), 7620.
- Hundhausen, A.: 1968, Direct observations of solar-wind particles. *Space Sci. Rev.* **8**(5–6), 690. DOI
- Huttunen, K.E.J., Koskinen, H.E., Schwenn, R.: 2002, Variability of magnetospheric storms driven by different solar wind perturbations. *J. Geophys. Res.* **107**(A7), SMP 20-1. DOI
- Isavnin, A., Vourlidas, A., Kilpua, E.: 2013, Three-dimensional evolution of erupted flux ropes from the sun (2–20 r) to 1 AU. *Solar Phys.* **284**(1), 203. DOI
- Kaiser, M.L., Kucera, T.A., Davila, J.M., St. Cyr, O.C., Guhathakurta, M., Christian, E.: 2008, The STEREO mission: An introduction. *Space Sci. Rev.* **136**, 5. DOI
- Kilpua, E., Pomoell, J., Vourlidas, A., Vainio, R., Luhmann, J., Li, Y., Schroeder, P., Galvin, A., Simunac, K.: 2009, STEREO observations of interplanetary coronal mass ejections and prominence deflection during solar minimum period. *Ann. Geophys.* **27**, 4491. DOI
- Kilpua, E., Jian, L., Li, Y., Luhmann, J., Russell, C.: 2011, Multipoint ICME encounters: Pre-STEREO and STEREO observations. *J. Atmos. Solar-Terr. Phys.* **73**(10), 1228.
- Klein, L.W., Burlaga, L.F.: 1982, Interplanetary magnetic clouds at 1 AU. *J. Geophys. Res.* **87**, 613. DOI
- Lepping, R.P., Burlaga, L.F., Jones, J.A.: 1990, Magnetic field structure of interplanetary magnetic clouds at 1 AU. *J. Geophys. Res.* **95**, 11957. DOI
- Lepping, R., Acuña, M., Burlaga, L., Farrell, W., Slavin, J., Schatten, K., Mariani, F., Ness, N., Neubauer, F., Whang, Y., et al.: 1995, The WIND magnetic field investigation. *Space Sci. Rev.* **71**(1–4), 207. DOI
- Lepping, R.P., Berdichevsky, D., Szabo, A., Lazarus, A.J., Thompson, B.J.: 2002, Upstream shocks and interplanetary magnetic cloud speed and expansion: Sun, Wind, and Earth observations. In: Lyu, L.-H. (ed.) *Space Weather Study Using Multipoint Techniques*, COSPAR Colloq. Ser. **12**, Pergamon Press, Amsterdam, 87.
- Lopez, R.E., Freeman, J.W.: 1986, Solar wind proton temperature–velocity relationship. *J. Geophys. Res.* **91**(A2), 1701. DOI
- Luhmann, J., Curtis, D., Schroeder, P., McCauley, J., Lin, R., Larson, D., Bale, S., Sauvaud, J.-A., Aoustin, C., Mewaldt, R., et al.: 2008, STEREO IMPACT investigation goals, measurements, and data products overview. *Space Sci. Rev.* **136**(1–4), 117. DOI
- Nieves-Chinchilla, T., Colaninno, R., Vourlidas, A., Szabo, A., Lepping, R., Boardsen, S., Anderson, B., Korth, H.: 2012, Remote and in situ observations of an unusual Earth-directed coronal mass ejection from multiple viewpoints. *J. Geophys. Res.* **117**(A6), A06106. DOI
- Ogilvie, K., Chornay, D., Fritzenreiter, R., Hunsaker, F., Keller, J., Lobell, J., Miller, G., Scudder, J., Sittler Jr, E., Torbert, R., et al.: 1995, SWE, a comprehensive plasma instrument for the Wind spacecraft. *Space Sci. Rev.* **71**(1–4), 55. DOI
- Riley, P., Linker, J., Lionello, R., Mikić, Z., Odstrčil, D., Hidalgo, M., Cid, C., Hu, Q., Lepping, R., Lynch, B., et al.: 2004, Fitting flux ropes to a global MHD solution: A comparison of techniques. *J. Atmos. Solar-Terr. Phys.* **66**(15), 1321. DOI
- Rodriguez, L., Mierla, M., Zhukov, A., West, M., Kilpua, E.: 2011, Linking remote-sensing and in situ observations of coronal mass ejections using STEREO. *Solar Phys.* **270**(2), 561. DOI
- Ruffenach, A., Lavraud, B., Owens, M.J., Sauvaud, J.-A., Savani, N., Rouillard, A., Démoulin, P., Foullon, C., Opitz, A., Fedorov, A., et al.: 2012, Multispacecraft observation of magnetic cloud erosion by magnetic reconnection during propagation. *J. Geophys. Res.* **117**(A9), A09101.
- Subramanian, P., Lara, A., Borgazzi, A.: 2012, Can solar wind viscous drag account for coronal mass ejection deceleration? *Geophys. Res. Lett.* **39**(19), L19107.
- Tsurutani, B.T., Smith, E.J., Gonzalez, W.D., Tang, F., Akasofu, S.I.: 1988, Origin of interplanetary southward magnetic fields responsible for major magnetic storms near solar maximum (1978–1979). *J. Geophys. Res.* **93**, 8519. DOI
- Vourlidas, A., Colaninno, R., Nieves-Chinchilla, T., Stenborg, G.: 2011, The first observation of a rapidly rotating coronal mass ejection in the middle corona. *Astrophys. J. Lett.* **733**(2), L23. DOI
- Vršnak, B., Žic, T., Vrbanec, D., Temmer, M., Rollett, T., Möstl, C., Veronig, A., Čalogović, J., Dumbović, M., Lulić, S., et al.: 2013, Propagation of interplanetary coronal mass ejections: The drag-based model. *Solar Phys.* **285**(1–2), 295. DOI

- Wang, C., Du, D., Richardson, J.D.: 2005, Characteristics of the interplanetary coronal mass ejections in the heliosphere between 0.3 and 5.4 AU. *J. Geophys. Res.* **110**, 10107. [DOI](#)
- Wang, Y., Ye, P., Wang, S., Zhou, G., Wang, J.: 2002, A statistical study on the geoeffectiveness of Earth-directed coronal mass ejections from March 1997 to December 2000. *J. Geophys. Res.* **107**(A11), SSH 2-1. [DOI](#)
- Wang, Y., Shen, C., Wang, S., Ye, P.: 2004, Deflection of coronal mass ejection in the interplanetary medium. *Solar Phys.* **222**(2), 329. [DOI](#)
- Wang, Y., Xue, X., Shen, C., Ye, P., Wang, S., Zhang, J.: 2006a, Impact of major coronal mass ejections on geospace during 2005 September 7–13. *Astrophys. J.* **646**(1), 625.
- Wang, Y., Zhou, G., Ye, P., Wang, S., Wang, J.: 2006b, A study of the orientation of interplanetary magnetic clouds and solar filaments. *Astrophys. J.* **651**(2), 1245.
- Wang, Y., Chen, C., Gui, B., Shen, C., Ye, P., Wang, S.: 2011, Statistical study of coronal mass ejection source locations: Understanding CMEs viewed in coronagraphs. *J. Geophys. Res.* **116**(A4), A04104. [DOI](#)
- Wang, Y., Wang, B., Shen, C., Shen, F., Lugaz, N.: 2014, Deflected propagation of a coronal mass ejection from the corona to interplanetary space. *J. Geophys. Res.* **119**(7), 5117.
- Wang, Y., Zhou, Z., Shen, C., Liu, R., Wang, S.: 2015, Investigating plasma motion of magnetic clouds at 1 AU through a velocity-modified cylindrical force-free flux rope model. *J. Geophys. Res.* **120**, 1543. [DOI](#)
- Whang, Y., Liu, C., Chang, C.: 1966, A viscous model of the solar wind. *Astrophys. J.* **145**, 255.
- Wu, C.-C., Lepping, R.P.: 2002, Effects of magnetic clouds on the occurrence of geomagnetic storms: The first 4 years of Wind. *J. Geophys. Res.* **107**, 1314. [DOI](#)
- Yashiro, S., Gopalswamy, N., Michalek, G., St Cyr, O., Plunkett, S., Rich, N., Howard, R.: 2004, A catalog of white light coronal mass ejections observed by the SOHO spacecraft. *J. Geophys. Res.* **109**(A7), A07105. [DOI](#)
- Yurchyshyn, V.: 2008, Relationship between EIT posteruption arcades, coronal mass ejections, the coronal neutral line, and magnetic clouds. *Astrophys. J. Lett.* **675**(1), L49.
- Yurchyshyn, V., Abramenko, V., Tripathi, D.: 2009, Rotation of white-light coronal mass ejection structures as inferred from LASCO coronagraph. *Astrophys. J.* **705**(1), 426. [DOI](#)
- Zhang, J., Richardson, I., Webb, D., Gopalswamy, N., Huttunen, E., Kasper, J., Nitta, N., Poomvises, W., Thompson, B., Wu, C.-C., et al.: 2007, Solar and interplanetary sources of major geomagnetic storms ($Dst \leq -100$ nT) during 1996–2005. *J. Geophys. Res.* **112**(A10), A10102. [DOI](#)